Assignments of ^{19}F NMR resonances and exploration of dynamics in a long-chain flavodoxin

Taylor A. Varner[1], Nishya Mohamed-Raseek[1], Anne-Frances Miller[1]*

[1]Department of Chemistry, University of Kentucky, Lexington, KY 40506

Running title: ^{19}F NMR-detected dynamics in a long chain flavodoxin

*To whom correspondence should be addressed: Anne-Frances Miller, Department of Chemistry, University of Kentucky, Lexington KY 40506-0055 U.S.A. Email: afmill3r2@gmail.com Tel# (859) 257-9349.

Key words: ^{19}F NMR, Long-chain Flavodoxin, fluoro-tyrosine, Protein dynamics, Partner protein interactions.

ABSTRACT

Flavodoxin is a small protein that employs a non-covalently bound flavin to mediate single-electron transfer at low potentials. The long-chain flavodoxins possess a long surface loop that is proposed to interact with partner proteins. We have incorporated ^{19}F-labeled tyrosine in long-chain flavodoxin from *Rhodopseudomonas palustris* to gain a probe of possible loop dynamics, exploiting the presence of a Tyr in the long loop in addition to Tyr residues near the flavin. We report ^{19}F resonance assignments for all four Tyrs, and demonstration of a pair of resonances in slow exchange, both corresponding to a Tyr adjacent to the flavin. We also provide evidence for dynamics affecting the Tyr in the long loop. Thus, we show that ^{19}F NMR of ^{19}F-Tyr labeled flavodoxin holds promise for monitoring possible changes in conformation upon binding to partner proteins.

Flavodoxin (Fld) is a small, soluble electron transport protein found in bacteria, algae and archaea.[2] It contains a single noncovalently bound flavin cofactor, flavin mononucleotide (FMN) which enables Fld to act as an electron carrier. Flavodoxin often replaces iron sulfur cluster containing ferredoxins when iron is scarce.[5, 6]

Flavodoxin is an excellent subject for study as its usual acidic nature makes it highly soluble and its tight structure consisting of a central five-stranded-β-sheet surrounded by two α-helical layers makes it extremely stable.[5, 7, 8] In our experience, Fld tolerates temperatures in excess of 40 ºC for more than two hours at concentrations above 1 mM without precipitation. Additionally, the flavin cofactor makes this protein easy to monitor by optical methods.[9] Thus, Fld has served as the 'hydrogen atom of flavoproteins' in which new methodology has been advanced.[10-18]

Flavodoxin serves as carrier of single reducing equivalents, consistent with Fld's ability to accumulate in each of the three possible oxidation states of FMN, depending on the ambient potential. Oxidized (OX) Fld's FMN cofactor accepts an electron and a proton to attain the neutral semiquinone (SQ) state at potentials from -100 to -250 mV (but see [4]). Acquisition of an additional electron yields the hydroquinone (HQ) state at lower potentials, from -380 to -520 mV.[19, 20] Fld protein is able to tune the reduction midpoint potentials (*E*°s) of the FMN cofactor by stabilizing the SQ and destabilizing the HQ states.[5] During reduction from the OX state, the SQ state is stabilized by formation of a new hydrogen bond to a backbone carbonyl.[21-23] Conversely, aromatic residues, often Tyr or Trp, sandwich the

isoalloxazine ring and destabilize the HQ state via hydrophobic/π stacking effects.[5, 20, 24-26] the HQ state is also destabilized by nearby anionic side chains,[27, 28] resulting in a very low $E°_{SQ/HQ}$ values, below that of free FMN.[5] Flavodoxin utilizes the SQ/HQ couple to shuttle electrons between electron sources such as photosystem I [3] and partner proteins such as nitrogenase.[6, 29-31]

Flavodoxins can be divided into two classes. Long-chain Flds are found in algae and cyanobacteria, whereas short-chain Flds are found in Gram-positive bacteria.[2] Both long- and short-chain Flds are found in Gram-negative bacteria.[20, 32, 33] Long-chain Fld are characterized by the presence of a 22-residue loop that interrupts β-strand 5.[34] It is thought that this loop participates in binding to a partner protein or stabilizes the flavin binding region.[2, 35, 36] The FldA of *Rhodopseudomonas palustris* (*Rpa*FldA) is a long chain Fld with residues 116 through 136 contributing to the 20-residue long loop (numbered according to *Rpa*FldA). High conservation is seen in the residues at the end of the long loop including the Gly residue at position 136, which has a conservation score of 9 according to Consurf analysis of 250 sequences. Additionally, the Tyr at position 121 and Ser at position 126 have conservation scores of 9. However, other residues in this region are less than 50% conserved. A recent cryoelectron microscopy structure of photosystem I complexed with Fld shows that residue 124 in the long loop approaches one of the other components of the complex [3]. Thus, it will be valuable to have solution-state probes of interactions between FldA and other proteins.

^{19}F NMR is an exceptionally versatile technique for probing changes in chemical environment. It has been used to detect protein and nucleic acid conformational changes, changes in oxidation state, internal protein dynamics, protein-membrane interactions, ligand binding, and protein folding/misfolding (reviewed by [37, 38]). The most common method of fluorine incorporation is via the use of non-canonical

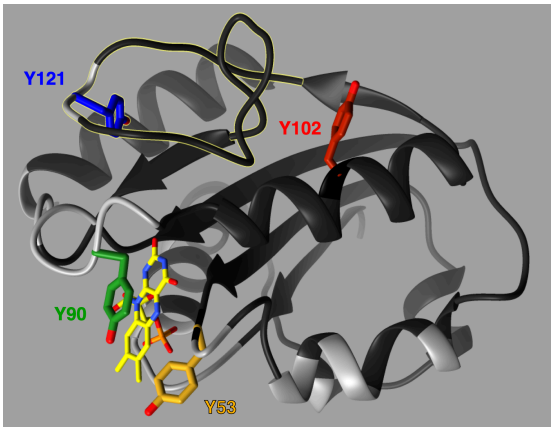

Figure 1: Ribbon diagram of *Rpa*FldA modeled on Ox *Avi*Fld (5K9B.pdb) showing the four labeled Tyrs in *Rpa*FldA.[1] The long loop is outlined in yellow (top left). The backbone ribbon is white for residues that interact with photosystem I.[3, 4]

fluorine-containing aromatic amino acids, although aliphatic and sulfur containing amino acids have also been utilized.[38] Fluorine incorporation tends not to disrupt protein structure, because F has a van der Waals radius of 1.4 Å, similar to that of hydrogen.[39, 40] ^{19}F-NMR benefits from a very low background because fluorine is virtually absent from biological systems. Nevertheless, ^{19}F has 100% isotopic abundance and is a spin ½ nucleus with 83% the strength of ^{1}H NMR.[37, 38, 41] This means that 1-dimentional (1D) ^{19}F NMR spectra yield strong signals allowing for lower-concentration samples. In addition to its many Goldilocks physical properties, ^{19}F-NMR is also extremely responsive to perturbations in chemical environment. Fluorine exhibits a chemical shift range of more than 400 ppm.[37, 42, 43] This responsiveness reflects shielding due to its exposed p-orbital electrons[42] and makes ^{19}F an ideal probe of biological molecules and processes.[44]

One of the challenges of studying flavin-containing proteins is the flavin's high molar absorptivity and ability to undergo photo-reduction. This complicates popular solution-based methods such as small angle Xray scattering (SAXs) or fluorescence resonance energy transfer (FRET) because the illumination involved can alter the

oxidation state of the flavin. Fluorine NMR eliminates this complication.

*Rpa*FldA is an ideal model for studying protein dynamics and changes in response to flavin oxidation state. It contains four Tyrs, able to report on regions of interest. Two of the Tyrs (Y53 and Y90) flank the flavin on either side, with Y90 π stacking with the flavin. Such a Tyr is expected to display broadening of its NMR signals upon reduction of the flavin to its semiquinone state, due to paramagnetic relaxation enhancement.[45] Y121 resides in the long loop making it an ideal candidate for monitoring dynamics of this region of the protein, and its possible participation in binding to partner proteins. In *R. palustris*, FldA is believed to accept an electron from the bifurcating electron transfer flavoprotein EtfAB and donate it to the Fe protein of nitrogenase.[6, 30, 46]

METHODS

Protein production. R. palustris FldA (*Rpa*FldA) was expressed in the NiCo21(DE3) strain of *Escherichia coli* (New England Biolabs Inc.) bearing a pET28b(+) derivative plasmid incorporating the gene for *Rpa*FldA under T7 control and fused to an N-terminal His_6 followed by a thrombin recognition sequence. The gene for *Rpa*FldA was constructed by Genscript based on the amino acid sequence RJF68323.1 reflecting *R. palustris* strain 1076. Low yields of fluorinated FldA were obtained from traditional M9 minimal medium.[47]. 3 L of bacterial culture yielded 0.25 x 10^{-6} moles of protein. Therefore a variant of the defined medium described by Muchmore *et al*. was used to increase protein yield.[48] Using this, 1 L of bacterial culture produced 0.5 x 10^{-6} moles of FldA = 9 mg. This constitutes a six-fold increase in protein yield.

10 mL of an initial overnight growth from a colony of the expression strain was used to inoculate 1 L of terrific broth (TB) medium supplemented with kanamycin at 0.1 mg/mL, and grown at 37 °C shaking at 200 rpm to an OD at 600 nm of 3. Cells from a 1 L culture in TB were harvested via centrifugation and then resuspended in 1 L of a half-strength version of the defined medium of Muchmore *et al*. lacking tyrosine but augmented with tryptophan (0.05 g / L) and kanamycin (0.1 mg/mL, Supporting Information). Cells were grown for 30 minutes at 37ºC and 200 rpm shaking in a 3 L baffled flask (Celltreat #229875), in order to exhaust metabolic pools of non fluorinated tyrosine. 170 mg/ L 3-fluoro tyrosine was then added and a second 30 minute interval at 37 °C, 200 rpm, was allowed to enable ^{19}F-tyrosine to permeate the metabolic pool, before induction with IPTG at 0.5 mM. The culture was grown for a further 16 hr. at 18 °C and 200 rpm agitation.

15 g bacterial cell paste were harvested via centrifugation and lysed via resuspension in 20 mL Bug Buster® (Millipore) in the presence of 1 mM free FMN, 1 µL benzonase nuclease (Millipore HC: 71205-3) and 1 µL rLysozyme (Millipore 71110-4) for 30 min. This mixture was centrifuged to separate soluble proteins from insoluble material Purification of soluble *Rpa*FldA utilized HisPur™ cobalt resin (Thermo Scientific) using the batch method of ThermoFisher in 20 mM 1,3-bis[tris(hydroxymethyl) methylamino]propane (bis-tris propane) pH 7.5 with 300 mM NaCl. HisPur™ resin that had been rinsed to remove storage buffer and equilibrated with the bis-tris propane buffer was mixed with the soluble proteins supernatant. The mixture was allowed to mix in a centrifuge tube on a tilt table for 1 hour at 4 °C. The mixture was then centrifuged at 700 rcf for 2 minutes and the supernatant was removed using a pipette so as to not disturb the resin bed. The resin was resuspended in 2 bed volumes of wash buffer (bis-tris propane buffer containing 20 mM imidazole, pH 7.5). The mixture was again centrifuged at 700 rcf for 2 minutes and the supernatant was removed with a pipette. This process was repeated until the supernatant was clear. The mixture was then resuspended in the elution buffer (bis-tris propane buffer containing 200mM imidazole, pH 7.5) and centrifuged as above. The supernatant containing the protein was

collected and concentrated using centricon tubes with 10 kD cutoff membranes. The concentrated protein was then run over a desalting column (10DG, BioRad #7322010) to remove any excess FMN. The His tag was not removed. Resulting protein was more than 90% pure based on sodium dodecyl sulfate polyacrylamide gel electrophoresis (Supporting Figure S1).

Mutations were designed based on a multiple sequence alignment of long-chain Flds wherein the most common alternative to Tyr was chosen to replace Tyr at each position. None of the long chain Flds had a residue other than Tyr at position 53 so Trp was used.

FMN content was quantified as in [49] wherein a sample of known FldA concentration at pH 7.5 was denatured by boiling for 5 minutes in darkness to release FMN, the solution was cleared by centrifugation and the FMN concentration was determined via the absorbance at 445 nm using the extinction coefficient of 12200 M^{-1} cm^{-1}.[50] Protein concentration was determined based on the Pierce™ 660nm protein assay relative to a BSA standard curve. Based on these values we obtained 1.2 ± 0.1 FMN per Fld (Supporting Table S4). At the relatively high concentrations of 2 - 0.1 mM used for NMR spectroscopy, FMN is not expected to dissociate significantly considering published dissociation constants below 1 nM [25, 51]. Moreover when we attempted to generate apo-FMN FldA by treating with 2 M KBr at pHs as low as 5.5, no FMN was removed. When we treated with 2M KBr in the presence of up to 8 M urea on a Ni column[52, 53] the recovered protein retained stoichiometric FMN but represented only half of the starting protein. Thus, our efforts indicate that FMN is very tightly bound to *Rpa*FldA at 1:1 stoichiometry and that apo-FMN *Rpa*FldA is not soluble. Therefore, any apo-FMN *Rpa*FldA that might be present in our preparations would be excluded from our NMR samples by our practice of centrifugation and passage over desalting columns to remove precipitate before loading protein into NMR tubes. Similarly, inclusion of excess FMN in the NMR samples made no difference to the spectra. Hence, our samples correspond to FMN-replete protein.

Electrospray mass spectrometry of *Rpa*FldA protein extracted into 50% water, 50% methanol and 0.1% formic acid employed direct infusion (5 µL / min) of the sample, but disrupted native structure and FMN binding so that the masses obtained represent the protein alone (lacking the N-terminal Met). Obtained masses indicated that the most abundant form of the protein incorporated four ^{19}F atoms in place of four H atoms, consistent with incorporation of 3F-Tyr in all four Tyr positions (Supporting Table S5 and Figure S2). To specify fluorinated *Rpa*FldA, we use the notation ^{19}F-*Rpa*FldA.

Reductive titrations were performed on non-fluorinated and fluorinated *Rpa*FldA in an inert atmosphere, monitored using a HP 8452A spectrophotometer (Agilent technologies) equipped with an OLIS controller, inside a glove box (Belle Technology, Waymouth, UK), using a 1 cm path length self-masking quartz cuvette at room temperature. 22.8 µM of FldA was reduced by small aliquots of Ti(III)Citrate (ε_{340} = 0.73 mM^{-1} cm^{-1}).[54]

Determination of the reduction midpoint potential of the OX/SQ redox couple ($E°_{OX/SQ}$). All midpoint potentials are quoted vs. NHE (normal hydrogen electrode). Spectro-electrochemical titrations were monitored optically as above, at 25 °C. Xanthine oxidase in combination with xanthine were used to provide a slow continuous delivery of reducing equivalents. The reaction mixture contained 400 µM xanthine, 10 µM methylviologen (mediator), 28 µM flavodoxin in working buffer (20 mM bis-tris propane, 300 mM NaCl at pH 7.5) along with 11.7 µM phenosafranin (PS, ε_{520} = 29 mM^{-1} cm^{-1}) as a reference dye ($E°$ = calculated to be −267.0 mV at pH 7.5 based on the $E°'$ of -252 mV NHE [55]). The reaction was initiated by addition of 12 nM xanthine oxidase, and spectra were recorded every 1 min. $E^{o}_{OX/SQ}$ was calculated by relating the extent of reduction of *Rpa*FldA to the extent of concurrent reduction of the PS. Conversion of *Rpa*FldA OX to SQ was quantified based on absorbance changes at 404 nm, the dye

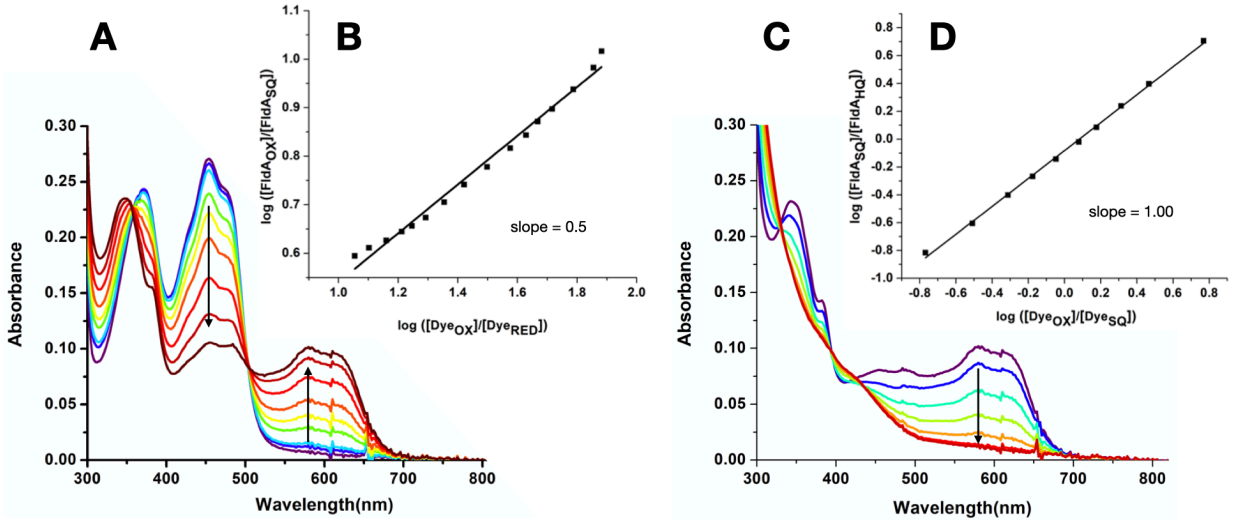

Figure 2: Reductive generation (A,B) and then consumption (C,D) of the SQ state of *Rpa*FldA, and associated *E*° determinations. Titrations were performed at pH 7.5 and 25 °C as described in the methods. The spectra shown were obtained without dyes present, to facilitate characterization of the states involved and the isosbestics and absorption maxima (A, C). Insets B and D show the log([FldA$_{oxidized}$]/[FldA$_{reduced}$]) associated with each transition vs. log([Dye$_{oxidized}$]/[Dye$_{reduced}$]). In panels A and B the two states of *Rpa*FldA are OX and SQ, and the best linear fit to the log/log data is y=0.50x -0.26. The reference dye was PS with an *E*° of -267 mV. In panels C and D the two states of *Rpa*FldA are SQ and HQ, and the best linear fit to the log/log data is y=1.00x -0.081. The reference dye was MV with an *E*° of -440 mV.

isosbestic. Reduction of the PS was quantified based on absorbance changes at 506 nm, an isosbestic point of *Rpa*FldA's OX/SQ couple.

Only spectra representing conversion of OX FldA to SQ were considered in this analysis. The onset of further reduction to *Rpa*FldA HQ co-occurred with reduction of the MV mediator so appearance of reduced MV• was taken to indicate attainment of potentials below which *Rpa*FldA SQ would be subject to further reduction. Each spectrum up to that point in the titration was converted to a difference spectrum by subtracting it from the initial spectrum, to reveal the extend of conversion of OX (positive) to SQ (negative). Absorbance at 404 nm (dye isosbestic) was used to find the absorbance change due to reduction of *Rpa*FldA and thereby to calculate the fraction of OX retained and SQ formed. [FldA$_{OX}$]/[FldA$_{SQ}$] at each point in the titration was calculated from these. A_{506} was used to calculate the extent to which oxidized dye, DYE$_{OX}$, was converted to reduced dye, DYE$_{RED}$. The ratio of oxidized to reduced dye along with that of the *Rpa*FldA were employed in the Nernst equation,

$$log\left(\frac{[\mathrm{FldA}_{OX}]}{[\mathrm{FldA}_{SQ}]}\right) = \frac{n_{FldA}}{n_{DYE}} log\left(\frac{[\mathrm{DYE}_{OX}]}{[\mathrm{DYE}_{RED}]}\right) + n_{FMN}\frac{F(E^{o}_{DYE} - E^{o}_{FldA})}{2.303RT}$$

where n_{FldA}, n_{DYE} denote the number of electrons acquired by the *Rpa*FldA flavin and the dye respectively during the reaction under study, and *F*, *R* and *T* are Faraday's constant, the ideal gas constant and the temperature, respectively. Spectra diagnostic of conversion of the OX state to the SQ, followed by conversion of SQ to HQ demonstrated that n_{FldA} = 1. A plot of $log\left(\frac{[\mathrm{FldA}_{OX}]}{[\mathrm{FldA}_{SQ}]}\right)$ versus $log\left(\frac{[\mathrm{DYE}_{OX}]}{[\mathrm{DYE}_{RED}]}\right)$ was then used to determine n_{FldA} from the known value of n_{DYE} = 2. The intercept of the plot then permitted calculation of $E°_{FldA}$ which in this case was the $E°_{OX/SQ}$ of *Rpa*FldA.

Determination of the $E°_{SQ/HQ}$ of RpaFldA. Reduction of *Rpa*FldA SQ occurred at a considerably lower potential, concurrent with reduction of MV (*E*° = −440 mV at pH 7.5).[56] The xanthine/xanthine oxidase system potential (near -345 mV)[57] was not low enough to reduce the *Rpa*FldA SQ. Therefore, Ti(III)citrate was used as the reductant (*E*°′ near -700 mV [58]). The reaction mixture contained 40 μM *Rpa*FldA

and 20 μM of MV, and was first reduced with addition of Ti(III)citrate[46] amounting to 30 μM (10 μM change per addition x 3) to reduce *Rpa*FldA OX, and then reduced more gradually with aliquots each increasing added Ti(III) citrate by 4 μM, until full reduction of MV was observed based on its absorption maximum at 396 nm (ε_{396} = 41.1 mM^{-1} cm^{-1}).[59]

A_{732} and A_{396} were used to calculate the extent to which the dye, was present as its SQ (MV•, the reduced state of the couple in effect) in each spectrum. The contribution of MV• was subtracted from each spectrum to yield spectra attributable to *Rpa*FldA SQ and HQ alone. In these, absorbance at 580 nm was used to quantify SQ remaining and thereby to calculate $[FldA_{SQ}]/[FldA_{HQ}]$ at each point in the titration. The ratio of oxidized dye (MV_{Tot} minus MV•) to reduced dye (MV•) along with the analogous ratio for FldA were employed in the Nernst equation, as described above, to obtain n_{FldA} and $E°_{SQ/HQ}$.

NMR spectroscopy. NMR samples were buffered with 20mM bis-tris propane pH 7.5, 200mM KCl and 10-12% D_2O unless otherwise stated. Samples requiring anaerobic conditions were prepared under nitrogen in a Belle box. For the Y121F and Y102H variants, the samples contained 1 mM FMN as a precaution to favour holo-FMN over apo-FMN *Rpa*Fld.

^{19}F NMR spectra were collected at 376 MHz using a Varian *Unity/Inova* 400MHz spectrometer at room temperature of 24 °C unless otherwise noted. T_1 values were measured for ^{19}F-*Rpa*FldA, the longest of which was 630 ms. 10.3 ppm-wide spectra were collected with a 45° excitation pulse, a 271ms acquisition time and a 800 ms recovery delay between transients. Spectra represented the average of 2048 transients for 2 mM protein (up to 36000 scans for 0.12 mM proteins, or 10 hours). Spectra were processed using backward linear prediction over the first 3 complex points and apodization using a 26 ms Gaussian, implemented in VnmrJ. Linewidths were determined via measurements of the peak half-widths at half height, wherein the side of the peak not subject to overlap could be used as a basis for the calculation.

The 2D EXSY spectrum was collected using a 400 ms mixing time, an acquisition time of 0.267 s, 3.1 s recovery delays between transients and spectral widths of 3896 Hz in both dimensions. 320 transients were averaged per scan. A 26 ms Gaussian window function was applied prior to four-fold zero-filling and Fourier transformation of the directly-detected dimension. 96 complex points were collected in the indirect dimension, doubled by linear prediction, subjected to a 24 ms Gaussian window

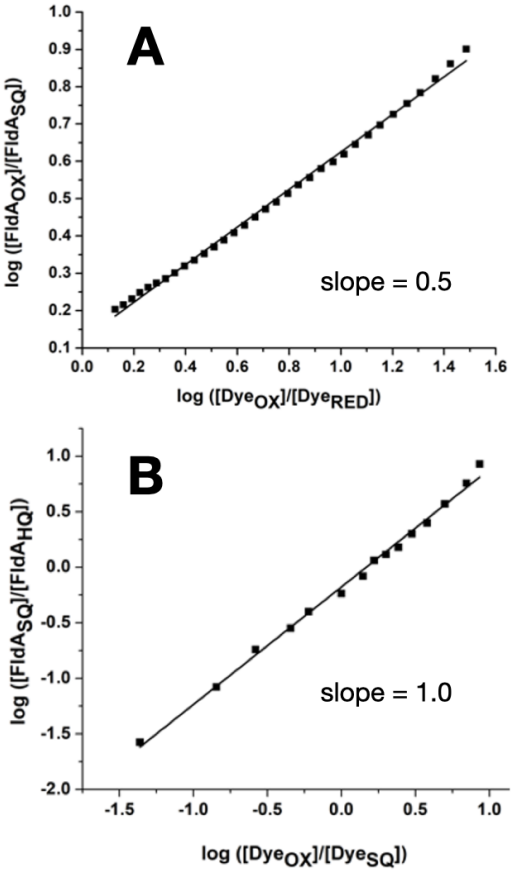

Figure 3. *E*° determinations for FldA incorporating ^{19}F in Tyr at a rate of ≈0.76. Titrations were performed at pH 7.5 and 25 °C as described in the methods. Panels A and B show the $\log([FldA_{oxidized}]/[FldA_{reduced}])$ associated with each transition *vs.* $\log([Dye_{oxidized}]/[Dye_{reduced}])$. In A: the OX/NSQ transition's best linear fit to the log/log data is y=0.50x +0.14, and in B, the NSQ/HQ log/log line is best described by y= 1.05x -0.169.

function and zero filled to 512 complex points prior to Fourier transformation.

To generate the SQ state, without loss of material or exposure to air, a degassed 0.6 mL OX sample was titrated with 30 µL of 70 mM Ti(III) citrate[54, 60] in Tris Buffer at pH 7 and the colour change monitored by eye and cell phone photos (see Supporting Figure S3).

Structural models were obtained using Swiss-Model[61, 62] based on each of the two crystal structures with the highest homology to the *Rpa*FldA amino acid sequence: 1OFV.pdb ([63] Fld from *Synechococcus elongatus*, previously called *Anacystis nidulans*) and 1YOB.pdb and 5K9B.pdb Fld from *Azotobacter vinelandii* [1, 20]. Both have sequence identify with *Rpa*FldA of 44% and similarity of more than 57% over more than 95% of their sequences. The resulting models were equivalent, the one based on *A. vinelandii* is referred to (Figure 1).

Results

Reduction midpoint potentials: Stepwise reduction of *Rpa*FldA at pH 7.5 revealed formation of the neutral (blue) SQ state, based on the strong absorbance between 550 and 650 nm (Figure 2A). Co-reduction with PS at pH 7.5 yielded a linear log/log plot of slope 0.5 as expected for a one-electron reduction of FldA vs. a two-electron reduction of PS (Figure 2B). The intercept of the line yielded $E°_{OX/SQ}$ = -271 mV ± 3 mV (2 independent determinations). Upon accounting for uptake of one proton per electron, we obtain $E°'$= -241 mV, which is similar to the $E°'$ of -221 mV obtained for the Fld of *S. elongatus* (*Sel*Fld) [56] and well within the -170 to -250 mV range of most long-chain Flds. $E°'_{OX/SQ}$ of short-chain Flds tend to be higher [20].

Stepwise reduction of *Rpa*FldA SQ was achieved used Ti citrate (Figure 2C),[46] and co-reduction with MV yielded a log/log plot with a slope of 1.002, matching the ideal value of 1.0 (Figure 2D). The intercept yielded $E°_{SQ/HQ}$ = - 434 mV ± 1 mV at pH 7.5 (2 independent determinations). Because no proton uptake is involved in forming anionic HQ from neutral SQ, this value is also the $E°'$, which compares extremely well with the value of -442 mV obtained for *Sel*Fld [56] and falls within the -415 to -465 mV range of most long-chain Flds [56]. Thus the thermodynamic landscape of *Rpa*FldA is unremarkable, making it a good model for long-chain Flds in general.

Table 1: E°s of fluorinated and non-fluorinated *Rpa*FldA.[a]

E° → Protein↓	OX/NSQ (mV)[b]	NSQ/HQ (mV)[b]
Native WT	-271 ± 3 (E°' = -241)	-434 ± 1
^{19}F-WT	-274 ±0.5 (E°' = -244)	-428 ±1.7
Reference dye	phenosafranine −267 mV [55]	methylviologen -440 mV [56]

[a] Measurements conducted at pH 7.5 in 20 mM bis-tris propane with 300 mM NaCl. Each measurement was repeated two times.
[b] All values quoted vs NHE

Incorporation of ^{19}F-Tyr resulted in most of the purified *Rpa*FldA being fluorinated at all four tyrosine residues, based on the strongest peak in the mass spectrum's having a mass 4x18 mass units larger than that of non-fluorinated *Rpa*FldA, which in turn was within one mass unit of the predicted value (see Supporting Information, Figure S2). Because the flavin is flanked on both sides by Tyr, we were curious as to whether fluorination could affect the $E°$s. The log/log plots corresponding to both

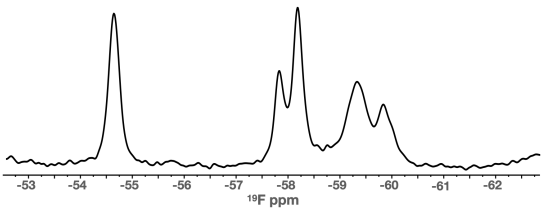

Figure 4. ^{19}F 1D NMR spectra of ^{19}F-*Rpa*FldA. 1 mM ^{19}F-*Rpa*FldA, 20mM Bis-tris propane, 200 mM KCl, pH 7.5. Deconvoluted peaks had relative areas of 1.03 : 0.49 : 0.94 : 1.02 : 0.60 (left to right).

transitions were both linear for ^{19}F-*Rpa*FldA (Figure 3), and the resulting *E°*s are compared with those of non-fluorinated *Rpa*FldA in Table 1. Changes were very small, on the order of uncertainty. Thus it appears that fluorination of the Tyr residues does not disrupt the redox reactivity of *Rpa*FldA. ^{19}F NMR studies were therefore pursued.

5 resonances for 4 tyrosines. 1D NMR spectra of ^{19}F-*Rpa*FldA produced based on *3*-^{19}F-tyrosine (^{19}F-Tyr) -containing medium revealed discrete ^{19}F NMR signals in the expected spectral region, confirming incorporation of this amino acid (Figure 4).[64] The resonances were adequately dispersed, demonstrating that each of the ^{19}F-Tyr residues has a chemical environment that is distinct enough to be distinguished from the others by ^{19}F NMR. All of the peaks were broad in comparison to ^{19}F signals from free ^{19}F-Tyr, as expected due to *Rpa*FldA's 17.7 kDa size. However, the spectrum displayed *five* resonances despite *Rpa*FldA's possession of only four tyrosine residues.

The peak intensity ratios of approximately 1.0 : 0.5 : 0.9 : 1.0 : 0.6 suggested that the peaks with areas of 0.5 and 0.6 at -57.8 and -59.8 ppm, respectively, might reflect alternative conformations affecting one of the ^{19}F-Tyr side chains. The crystal structure of *Bacillus cereus* Fld revealed co-population of two conformations of the so-called '50s' backbone loop that hydrogen bonds (H-bonds) to flavin, at a residue adjacent to one of our Tyr residues, providing one possible explanation.[65] However the fact that the two smaller peaks were almost equal in size also suggested that they might reflect the two positions possible for ^{19}F if a single rotamer of the ^{19}F-Tyr side is not able to rotate on the timescale of the chemical shift difference.[66]

We tested whether the larger number of resonances than residues could reflect a ^{19}F-Tyr side chain that populates two slowly-interconverting conformations. Given the 2 ppm separation between the two half-strength peaks, an exchange rate lower than $2\pi*2*376$ Hz = 4.7 x 10^3 s^{-1} is required[67] whereas more rapid conformational

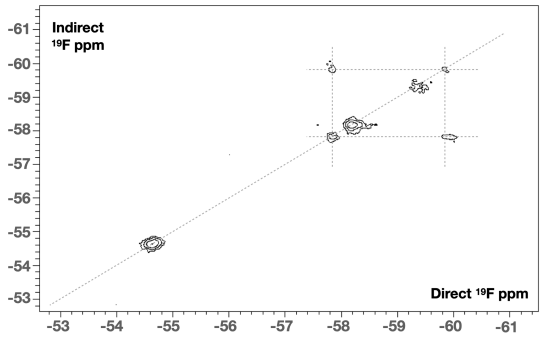

Figure 5: 2D EXSY of ^{19}F-*Rpa*FldA. 1 mM ^{19}F-*Rpa*FldA was used along with a 400 ms mixing time. Details are in the methods section.

exchange exposes the ^{19}F probe to a single average environment.[68] If the postulated slow exchange rate is nonetheless greater than $1/\tau$ where τ is the duration of a mixing time, then exchange between environments can occur within the mixing time and be manifested by cross-peaks in a 2D Exchange Spectroscopy (EXSY) NMR experiment.[69] Figure 5 shows that this is indeed the case for ^{19}F-*Rpa*FldA at room temperature.

The EXSY spectrum of ^{19}F-*Rpa*FldA displayed a pair of symmetry-related cross peaks revealing chemical exchange between resonances at -57.8 and -59.8 ppm. The possibility that the cross-peaks represented an nOe between two different ^{19}F atoms is less likely because the two peaks connected were precisely those with half-intensity each. If the cross-peaks represent chemical exchange, the latter would need to occur with a rate greater than 2.5 s^{-1}, but this is compatible with the upper limit implied by the peak separation. Based on saturation transfer buildup, we estimate a conformational exchange rate of 3 - 13 s^{-1} (Supporting Information Figure S4 and Table S6).

Assignment of the resonances. A second test of the chemical exchange interpretation was conducted by site-directed mutagenesis of the *Rpa*FldA gene. We hypothesized that if a single ^{19}F-Tyr was responsible for both half-strength resonances, then both should be absent from a variant in which that one Tyr was

converted to another amino acid. Each of the four Tyrs was replaced in turn, to test possible identities for the residue in question, and also to obtain site-specific assignments of the NMR signals.

We generated the Y53W, Y90W, Y102H, and Y121F variants for *Rpa*FldA, basing our choice of replacement amino acid on identities observed at the same position in homologous Flds. The Y53W variant proved to have low solubility and accumulated in the pellet obtained after rupturing cells and centrifugation. As a result, data from this variant are not reported. The Y90W variant had the greatest stability with the highest yield. Figure 6 shows that the resonances at -57.8 and -59.8 are both attributable to Y90 (Tyr90) because both are absent from the Y90W variant but not affected in any other. This confirms that these two signals represent distinct conformations affecting Y90.

NMR spectra of other variants permit assignment of the resonances affected (Table 2). By process of elimination, the prominent down-field resonance at -54.6 ppm can be assigned to residue Y53.

Table 2: Summary of ^{19}F peak assignments

Chemical Shift[a] (ppm)	Assign-ment[b]	T_1 (s)[c]	Relative Area[d]
-54.64	Y53	0.488 ±.009	1.03
-57.81	Y90 a	0.63 ± .06	0.49
-58.19	Y102	0.43 ± .02	0.94
-59.37	Y121	0.32 ± .01	1.02
-59.82	Y90 b	0.53 ± .03	0.60

[a] Relative to external neat trifluoroethylene.
[b] Two resonances are attributed to Y90 so their labels are augmented by 'a' or 'b'.
[c] Uncertainties are standard error of fits.
[d] Due to peak overlaps, areas were determined after implementing a Lorentzian deconvolution, in Agilent's VnmrJ software.

Sensitivity to flavin oxidation state. The assignment to Y90 of the two resonances in chemical exchange is particularly interesting as this residue is conserved as a Tyr or Trp residue in other long-chain Flds and most structures show it to be stacked against the

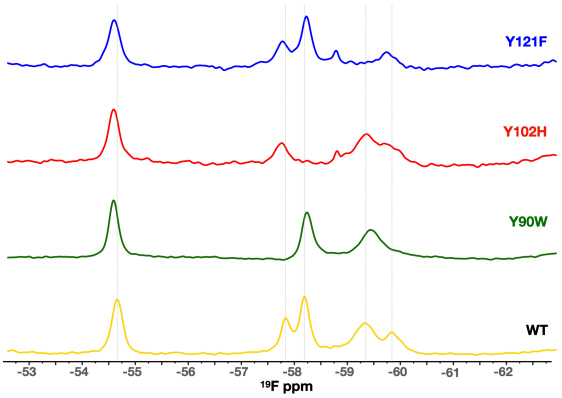

Figure 6: 1D NMR spectra of fluorinated WT 0.5 mM WT *Rpa*FldA 20 mM bis-Tris propane, 200 mM KCl, pH 7.5, 0.18 mM Y90W FldA, 0.14 mM Y102H FldA, 0.12 mM Y121F FldA. All three mutants were in 20mM bis-Tris propane, 300mM NaCl, pH 7.5. Y102H & Y121F contained 1mM free FMN to suppress apoprotein.

flavin isoalloxazine ring. To test whether this is true in ^{19}F-*Rpa*ETF as well, and thereby our structural model (Figure 1), we chemically reduced the protein to populate its SQ state. Because this would produce a free radical centered on the flavin, we expected broadening and even obliteration of the resonances of ^{19}F atoms nearby.

Figure 7 compares NMR spectra of OX and SQ ^{19}F-*Rpa*FldA. As expected, the resonance we assigned to Y53 is visibly broadened, consistent with its position flanking the flavin (Figure 1). The resonance attributed to Y90 at –57.8 ppm disappeared altogether (Y90a), indicating that one of the conformations of Y90 places it even closer to

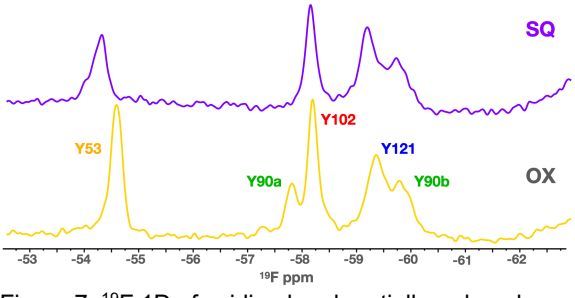

Figure 7: ^{19}F 1D of oxidized and partially reduced ^{19}F-*Rpa*FldA. 1 mM OX ^{19}F-*Rpa*FldA (yellow) is compared with 2.2 mM ^{19}F-*Rpa*FldA that had been partially reduced using Ti(III) citrate, in a glove box. Full formation of the SQ was not achieved without precipitation; the spectrum shown represents a sample that had become teal blue in colour indicating substantial SQ formation (estimated at 75%).

the flavin (the 'a' conformation). This is agreement with crystal structures showing a variety of orientations and placements of the Y53 ring (Supporting Figure S5), in contrast to well-defined stacking for Y90 in most crystal structures. Also, replacement of Y90 weakens FMN binding more than does replacement of Y53, consistent with the larger effect of paramagnetism on Y90a.[51] Interestingly, the resonance of Y90's b conformation at -59.8 ppm was not changed in amplitude, chemical shift or breadth, arguing that the b conformation places Y90 further from the flavin than Y53, and that reduction of the flavin does not significantly alter the relative populations of the a and b conformations .[65] We note that the 90b resonance was relatively broad even in the absence of paramagnetism, but its persistence when the companion 90a resonance was fully relaxed requires that the conformational exchange rate be lower that the rate of paramagnetically enhanced relaxation (PRE).

Residues Y102 and Y121 are further away from the flavin based on our model. Although *Rpa*FldA is only 17.7 kDa, the distance between these residues and the flavin radical seem to be sufficient to limit paramagnetic line broadening to a contribution that is small compared to the natural line width. In this connection, we note that PRE drops off as the inverse sixth power of the distance, so a 12% increase in distance from the flavin would halve the paramagnetic contribution to line width.[70, 71] Thus, Y90 need not move very far to allow the population in the b conformation to remain detectable.

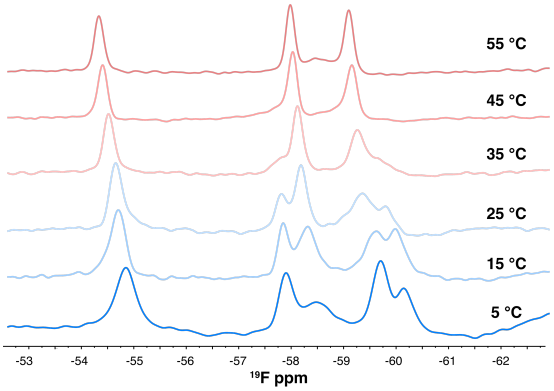

Figure 8: Temperature Dependence of the ^{19}F 1D NMR of 0.5 mM ^{19}F-*Rpa*FldA in 20 mM Bis-Tris propane, 200 mM KCl, pH 7.5.

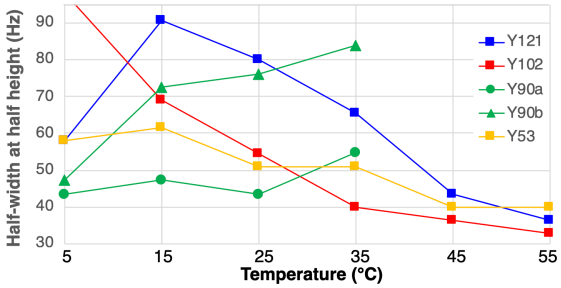

Figure 9. Temperature dependence of resonance widths. Resonance half-widths at half height are plotted. The colour-code used conforms to the colouring in Figure 1.

Evidence for internal dynamics. Since the EXSY result and the effect of replacing Y90 both support two conformations as the origin of the peaks at -57.8 and -59.8 ppm, but the PRE of only one resonance indicates slow exchange that involves positions different distances from the flavin, we further tested the hypothesis that Y90 is in slow conformational exchange. We varied the temperature with the expectation that the Y90a and Y90b resonances should converge and broaden at higher temperatures, in contrast with resonances with linewidths determined by overall molecular tumbling, which should become more narrow at higher temperatures. The data in Figure 8 bear out these predictions: the resonances of Y53, Y102 and Y121 sharpened as the temperature was raised, however the resonances attributed to Y90 broadened (Figure 9).

The two resonances we assigned to Y90 also approached one another as the temperature was raised, and appear to have coalesced at 55 °C. Estimating the coalescence temperature to be 50 °C and the low-temperature limit of the peak separation to be 2.26 ppm * 376 MHz * 2π = 5.34 kHz, we estimate a chemical exchange rate of $k_{ex} = (\omega_A - \omega_B)/2\sqrt{2}$ = 1.89 x 10^3 s^{-1} applicable at 50 °C.[67] Even given considerable slowing at 25 °C, this allows for the cross peaks observed in the EXSY to be attributed to chemical exchange.

At 25 °C the resonance of Y121 appears to very broad (-59.4 ppm) but appears to sharpen at the lowest temperature suggesting a coalescence temperature near 25 °C and a minority population resonating at less negative chemical shifts (possibly in the envelope of Y102's low-temperature resonance near -58.5 ppm). We do not attribute these changes in line width to flavin paramagnetism, because of the sharpening at lower temperature, and because it was observed in samples that were fully oxidized. Without knowing the separation between the related resonances at the slow-motion limit, it is not possible to estimate the conformational exchange rate that applies.[67] Thus, the dynamics of Y121 and Y90 could be reflections of the same event, or different ones. Regardless, ^{19}F NMR supports proposals that alternate conformations in the long loop could exist in free vs. bound Fld.[3, 35]

Discussion

Our data address novel dynamics that have begun to emerge from studies of interactions between Fld and partners, via our signals from Y90 and Y121.[3, 35] However our data also inform on the long-recognized '50s loop' via the signal from Y53.[22] Conformation change coupled to flavin reduction was demonstrated more than four decades ago[8] when several different Flds were shown to adopt a different backbone conformation near the flavin N5 upon flavin reduction.[22] While a backbone NH in the '50s loop' *donates* a H-bond to the flavin N5 when the flavin is OX, reduction of the flavin to neutral SQ (NSQ) is associated with a backbone flip whereupon the preceding residue's carbonyl O *accepts* an H-bond from the flavin N5H, thereby stabilizing the NSQ state and raising the associated $E°_{OX/SQ}$.[56, 72, 73] (Flavin numbering provided in Supporting Figure S6.)

In our ^{19}F-*Rpa*FldA, the Y53 resonance reporting on the 50s loop is in the fast exchange regime throughout the temperature range covered This unites with measurements of binding affinity[51, 74] to indicate weak interactions between the side chain of Y53 and the OX flavin ring system. The lack of effect on the flavin E°s upon fluorination of Tyr is consistent with this, in addition to incomplete fluorination.

Many of the Flds studied possess a Gly at the position whose carbonyl O accepts a H-bond. The *Sel*Fld has an Asn there, but replacement of Asn58 by Gly raises the $E°_{OX/SQ}$ consistent with a diminished cost of re-orienting the backbone (*Sel*Fld numbering) [56]. *Rpa*FldA's analogous position is G54 so Y53 is positioned to report on this stretch of backbone. *Rpa*FldA's $E°'_{OX/SQ}$ of -198 mV compares well with the $E°'_{OX/SQ}$ of N58G *Sel*Fld of -175 mV.[56] The value for *Avi*Fld is also higher than ours at -157 mV [1] although it resembles *Rpa*FldA in possessing a Gly at position 54 (*Rpa*FldA numbering), thus as-yet unexplored distinctions between *Rpa*FldA and its nearest homologues appear to modulate the $E°_{OX/SQ}$.

The physiologically relevant couple is the SQ/HQ equilibrium. $E°_{SQ/HQ}$s of long-chain Flds range between -370 and -520 mV, very low for a flavin.[20, 56] This has been attributed to formation of anionic HQ in the presence of anionic amino acid side chains, in the Flds of *Desulfovibrio vulgaris* [27, 28, 75] *Clostridium beijerinckii,*[22] *Anabaena* [25, 76] and *Megasphaera elsdenii*.[75, 77] The anionic residues which are held responsible in *Sel*Fld [27, 28] are conserved in *Rpa*FldA as well. *Rpa*FldA's $E°'_{SQ/HQ}$ of -434 mV is close to that of *Sel*Fld ($E°'_{SQ/HQ}$ = -442 mV [56]) but significantly higher than that of similarly closely related *A. vinelandii* Fld (*Avi*Fld, $E°_{SQ/HQ}$ at pH 7.5 of -483 mV [1], which also retains the two Asp residues in question). It has been pointed out that hydrophobic π stacked residues flanking the flavin would tend to maintain a low dielectric around it and thus destabilize the anionic HQ (lowering $E°_{SQ/HQ}$).[25] This is particularly significant as novel Flds emerge that lack the constellation of anionic side chains, but retain the low $E°_{SQ/HQ}$.[4] *Rpa*FldA possesses a Tyr (Y53) where *Sel*Fld

possesses a Trp and *Avi*Fld has a Leu. On the other face of the flavin, all three have Tyr (Y90 in *Rpa*FldA). Overall, the *E*°s of *Rpa*FldA are consistent with those of related proteins, given the differences between them. Our finding that fluorination has insignificant effect on the E°s is surprising in this regard. Future studies will exploit the lowered pK_a of ^{19}F-Tyr relative to normal Tyr (8.4 vs. 9.9 [78]) to probe the effect of deprotonation of one of the Tyr flanking the flavin. The 50s loop reorientation associated with flavin reduction[72, 73] may factor into the chemical shift change observed for Y53 upon partial reduction.

The 90s loop and the long loop are represented in our data by Y90 and Y121, respectively. Y90 displays clear slow-exchange dynamics. Because our samples retain stoichiometric FMN and the resonance of the other flanking Tyr, Y53, lacks such an effect, we do not attribute it to slow interconversion of apo- and holo-FMN *Rpa*FldA. Because substitutions of Tyr residues elsewhere in the protein had limited effect on the phenomenon, we attribute it to a relatively local event rather than a global one, and interpret it to represent conformational change of one or both of the 90s loop and the long loop. These are adjacent to one-another so only one of the two need move to affect the chemical shifts of both Tyrs. Based on average B-factors per residue in the structure of *Avi*Fld, residues in the long loop are less conformationally restricted than those in the 90s loop, but both would gain more mobility in solution than the crystallographic structures depict (Supporting Figure S7).

Fast dynamics in solution have been addressed by NMR, via (^{1}H)-^{15}N nOes, ^{15}N T_1 and ^{15}N T_2. These indicate that the Trp58 indole ring of *Anabaena* Fld corresponding to Tyr53 was relatively rigid, on a ps-ns time scale.[79] However dynamics on a µs-ms time scale was found to affect the Tyr corresponding to our Tyr90, but not the Trp58 corresponding to our Tyr53, in the Fld from *D. vulgaris* (a short-chain Fld), based on ^{15}N T_1/T_2 values of backbone amides,[80] Thus there is precedent in solution studies for backbone dynamics in the 90s loop.

Y121 in the long loop might retain similar environments explaining the modest deviation from fast exchange we observe, whereas movement of Y90 that removes it from a π stack with flavin would have a larger effect on ^{19}F chemical shift, explaining its slow-exchange behaviour, despite a shared conformational exchange rate. The 90a resonance was sharper than that of 90b in all the variants, and 90a is the one affected by PRE, so we interpret 90a as reflecting the conformation of Y90 stacked on the flavin that is seen in so many crystal structures.[1, 3, 22, 63, 81, 82] Meanwhile, the greater breadth of the y90b resonance is consistent with a proposed 'open' conformation of the 90s loop in which the Tyr ring is less constrained.

Detachment of Y90 from the flavin would make it more accessible to electron transfer partners. Indeed, ferredoxin $NADP^+$ oxidoreductase and homologues provide a 'placeholder' Tyr, Trp or Phe sidechain that stacks on the flavin but makes way for substrate binding during turnover.[83] A recent cryo-electron microscopy structure of Fld in complex with photosystem I (PSI) shows a side chain from PSI forming an H-bond with the side chain OH of the Fld Tyr homologous to *Rpa*FldA Y90, while another PSI subunit H-bonds with the backbone of the residue homologous to Val88 of *Rpa*FldA, and a third contact with PSI engages the long loop. Fld residues in the 90s loop, including the homologue of Y90, were determined to participate in binding to physiological partner proteins,[84] and the 90s loop was also identified as having distinct conformations in the two participants in a Fld dimer from *Desulfovibrio gigas* Fld.[36] Thus this region appears able to adapt to partner proteins as part of binding.[3] Moreover the Gln16 of PSI that engages Fld's Y90 is itself two residues from the Cys14 ligand to the Fe_4S_4 cluster that donates an electron to the Fld flavin. Thus it is possible that conservation of an aromatic

side chain in Fld's position 90 also reflects a role in electron transfer.[85, 86]

Despite *Rpa*FldA's having only four Tyrs, the rich information content in the ^{19}F NMR spectrum of ^{19}F-*Rpa*FldA promises to be useful for studying interactions with its partner proteins. Having assigned the signals of each of the Tyrs we are now in a position to determine what regions of *Rpa*FldA are most responsive to association with EtfAB and therefore may participate in binding to it. Specifically, we will test the hypothesis that the long loop will be affected.[3, 35]

Author Contributions

TAV wrote much of the first draft and collected all NMR data, NMR executed the spectro-electrochemistry and provided the associated methods, AFM analyzed the temperature dependence and saturation transfer, and produced the submitted versions of the manuscript. All authors contributed figures and commented on the manuscript.

Declaration of competing interests

The authors declare they have no conflicts of interest.

Acknowledgments

We are honoured to have had the support of the National Science Foundation under CLP1808433 and the University of Kentucky's office of the vice president for research in the form of an IRC pilot grant. We thank Hunter Mulloy for assistance with SDS-gels and Dallas M. Bell for help with protein production and purification. This work is partially supported by DOE-EPSCoR grant DE-SC0021283.

References

[1] H.M. Segal, T. Spatzal, M.G. Hill, A.K. Udit, D.C. Rees, Electrochemical and structural characterization of *Azotobacter vinelandii* flavodoxin II., Prot. Sci. 26 (2017) 1984-1993.
[2] P. Karlusich, A.F. Lodeyro, N. Carrillo, The long goodbye: the rise and fall of flavodoxin during plant evolution., J. Exp. Botany 65(18) (2014) 5161-5178.
[3] P. Cao, D.F. Cao, L. Si, X.D. Su, W.R. Chang, Z.F. Liu, X.Z. Zhang, M. Li, Structural basis for energy and electron transfer of the photosystem I-IsiA-flavodoxin supercomplex., Nat.Plants 6 (2020) 167-176.
[4] D. Prakash, P.R. Iyer, S. Suharti, K.A. Walters, G.M. Santiago-Martinez, J.H. Golbeck, K.S. Murakami, J.G. Ferry, Structure and function of an unusual flavodoxin from the domain *Archaea.*, Proc. Nat. Acad. Sci. U S A 116(51) (2019) 25917-25922.
[5] J. Sancho, Flavodoxins: sequence, folding, binding, function and beyond, Cell. Mol. Life Sci. 63 (2006) 855-864.
[6] E. Knight, Jr., R.W.F. Hardy, Isolation and characteristics of flavodoxin from nitrogen-fixing Clostridium pasteurianum, J. Biol. Chem. 241(12) (1966) 2752-2756.
[7] K.D. Watenpaugh, L.C. Sieker, L.H. Jensen, Binding of riboflavin-5'-phosphase in a flavoprotein - flavodoxin at 2.0 Å resolution, Proc. Nat. Acad. Sci. U.S.A. 70(12) (1973) 3857-3860.
[8] R.D. Andersen, P.A. Apgar, R.M. Burnett, G.D. Darling, M.E. LeQuesne, M.L. Ludwig, Structure of the Radical Form of *Clostridial* Flavodoxin: A New Molecular Model, Proc. Natl. Acad. Sci. U S A 69 (1972) 3189-3191.

[9] A.F. Miller, H.D. Duan, T.A. Varner, N. Mohamed-Raseek, Reduction midpoint potentials of bifurcating electron transfer flavoproteins., Meth. Enzymol. 620 (2019) 365-398.
[10] S.J.O. Hardman, C.R. Pudney, S. Hay, N.S. Scrutton, Excited state dynamics can be used to probe donor-acceptor distances for H-tunneling reactions catalized by flavoproteins., Biophys. J. 105 (2013) 2549-2558.
[11] G. Kodali, S.U. Siddiqui, R.J. Stanley, Charge redistribution in oxidized and semiquinone E. coli DNA photolyase upon photoexcitation: Stark spectroscopy reveals a rationale for the position of Trp382., J. Am. Chem. Soc. 131 (2009) 4795-4807.
[12] D.P. Zhong, A.H. Zewail, Femtosecond dynamics of flavoproteins: charge separation and recombination in riboflavine (vitamin B-2)-binding protein and in glucose oxidase enzyme, Proc. Natl. Acad. Sci. U.S.A. 98 (2001) 11867-11872.
[13] T. Maly, D. Cui, R.G. Griffin, A.-F. Miller, Dynamic nuclear polarization based on an endogenous radical, J. Phys. Chem. -B 116 (2012) 7055-7065.
[14] D. Cui, R.L. Koder, Jr., P.L. Dutton, A.-F. Miller, ^{15}N Solid-State NMR as a probe of Flavin H-bonding., J. Phys. Chem -B. 115(24) (2011) 7788-7798.
[15] D.H. Murgida, E. Schleicher, A. Bacher, G. Richter, P. Hildebrandt, Resonance Raman spectroscopic study of the neutral flavin radical complex of DNA photolyase from Escherichia coli, J. Raman Spectrosc. 32 (2001) 551-556.
[16] K.-Y. Yang, R.P. Swenson, Nonresonance Raman Study of the Flavin Cofactor and Its Interactions in the Methylotrophic Bacterium W3A1 Electron-Transfer Flavoprotein, Biochem. 46 (2007) 2298-2305.
[17] P.K. Dutta, R. Spencer, C. Walsh, T.G. Spiro, Vibrational assignments and the zwitterionic structure of 8-methylamino-riboflavin., Biochim. Biophys. Acta 623 (1980) 77-83.
[18] G. Tollin, D.E. Edmondson, Flavoprotein chemistry. I. Circular dichroism studies of the flavine chromophore and of the relation between redox properties and flavine environment in oxidases and dehydrogenases., Biochemistry 10(1) (1971) 113-124.
[19] J. Deistung, R.N.F. Thorneley, Electron transfer to nitrogenase: Characterization of flavodoxin from *Azotobacter chroococcum* and comparison of its redox potentials with those of flavodoxins from Azotobacter vinelandii and *Klebsiella pneumoniae* (nifF gene product), Biochem. J. 239 (1986) 69-75.
[20] S. Alagaratnam, G. van Pouderoyen, T. Pijning, B.W. Dijkstra, D. Cavazzini, G.L. Rossi, W.M.A.M. van Dongen, C.P.M. van Mierlo, W.J. van Berkel, G.W. Canters, A crystallographic study of Cys69Ala flavodoxin II from *Azotobacter vinelandii*: Structural determinants of redox potential., Prot. Sci. 14 (2005) 2284-2295.
[21] P.A. O'Farrel, M.A. Walsh, A.A. McCarthy, T.M. Higgins, G. Voordouw, S.G. Mayhew, Modulation of the redox potentials of FMN in *Desulfovibrio vulgaris* flavodoxin: thermodynamic properties and crystal structures of glycine-61 mutants., Biochemistry 37 (1998) 8405-8416.
[22] M.L. Ludwig, K.A. Pattridge, A.L. Metzger, M.M. Dixon, M. Eren, Y. Feng, R.P. Swenson, Control of oxidation-reduction potentials in flavodoxin from *Clostridium beijerinckii*: the role of conformational changes, Biochemistry 36 (1997) 1259-1280.
[23] F.-C. Chang, R.P. Swenson, The midpoint potentials for the oxidized-semiquinone couple for Gly57 mutants of the *Clostridium beijerinckii* flavodoxin correlate with changes in the hydrogen-bonding interaction with the proton on N(5) of the reduced flavin mononucleotide

cofactor as measured by NMR chemical shift temperature dependencies., Biochemistry 38 (1999) 7168-7176.
[24] A.A. McCarthy, M.A. Walsh, C.S. Verma, D.P. O'Connel, M. Reinhold, G.N. Yalloway, D. d'Arcy, T.M. Higgins, G. Voordouw, S.G. Mayhew, Crystallographic investigation of the role of aspartate 95 in the modulation of the redox potentials of Desulfovibrio vulgaris flavodoxin., Biochemistry 41 (2002) 10950-10962.
[25] A. Lostao, C. Gomez-Moreno, S.G. Mayhew, J. Sancho, Differential stabilization of the three FMN redox forms by tyrosine 94 and tryptophan 57 in flavodoxin from *Anabaena* and its influence on the redox potentials, Biochemistry 36 (1997) 14334-14344.
[26] R.P. Swenson, G.D. Krey, Site-directed mutagenesis of Tyrosine-98 in the flavodoxin from *Desulfovibrio vulgaris* (Hildenborough): Regulation of the oxidation-reduction properties of the bound FMN cofactor by aromatic, solvent and electrostatic interactions., Biochemistry 33 (1994) 8505-8514.
[27] Z. Zhou, R.P. Swenson, Electrostatic effects of surface acidic amino acid residues on the oxidation-reduction potentials of the flavodoxin from *Desulfovibrio-vulgaris* (Hildenborough). Biochemistry 34 (1995) 3183-3192.
[28] Z. Zhou, R.P. Swenson, The cumulative electrostatic effect of aromatic stacking interactions and the negative electrostatic environment of the flavin mononucleotide binding site is a major determinant of the reduciton potential for the flavodoxin from *Desulfovibrio vulgaris* [Hildenborough]. Biochemistry 35 (1996) 15980-15988.
[29] V.K. Shah, G. Stacey, W.J. Brill, Electron transport to nitrogenase: characterization of pyruvate:flavodoxin oxidoreductase, the *nif*J gene product., J. Biol. Chem. 258 (1983) 12064-12068.
[30] K.R. Fixen, N.P. Chowdhury, M. Martinez-Perez, S. Poudel, E.S. Boyd, C.S. Harwood, The path of electron transfer to nitrogenase in a phototrophic alpha-proteobacterium, Env. Micro. 20(7) (2018) 2500-2508.
[31] J. Klugkist, H. Haaker, C. Veeger, Studies on the mechanism of electron transport to nitrogenase in *Azotobacter vinelandii*., Eur. J. Biochem. 155 (1986) 41-46.
[32] J. Sancho, S. Salillas, Flavodoxins as Novel Therapeutic Targets against Helicobacter pylori and Other Gastric Pathogens, Int. J. Mol. Sci. 21(5) (2020) 1881.
[33] S.G. Mayhew, G. Tollin, Flavodoxins and electron-transfer- ring flavoproteins., in: P.D. Boyer (Ed.), The Enzymes, Acad. Press, New York, 1992, pp. 57-118.
[34] E. Steensma, M.J.M. Nijman, Y.J.M. Bollen, P.A. De Jager, W.A.M. van den Berg, W.M.A.M. van Dongen, C.P.M. van Mierlo, Apparent local stability of the secondary structure of *Azotobacter vinelandii* holoflavodoxin II as probed by hydrogen exchange: Implications for redox potential regulation and flavodoxin folding,, Prot. Sci. 7 (1998) 306-317.
[35] J. López-Llano, S. Maldonado, M. Bueno, A. Lostao, M. Ángeles-Jiménez, M.P. Lillo, J. Sancho, The long and short flavodoxins I. The role of the differentiating loop in apoflavodoxin structure and FMN binding., J. Biol. Chem. 279(45) (2004) 47177-47183.
[36] Y.-C. Hsieh, T.S. Chia, H.-K. Fun, C.-J. Chen, Crystal structure of dimeric flavodoxin from Desulfovibrio gigas suggests a potential binding region for the electron-transferring partner. , Int. J. Mol. Sci. 14(1) (2013) 1667-1683.
[37] E.N.G. Marsh, Y. Suzuki, Using ^{19}F NMR to Probe Bilogical Interactions of Proteins and Peptides, ACS Chem. Biol. 9 (2014) 1242-1250.

[38] J.L. Kitevski-LeBlanc, R.S. Prosser, Current applications of ^{19}F NMR to studies of protein structure and dynamics., Prog. Nucl. Magn. Reson. Spec. 62 (2012) 1-33.
[39] M. Salwiczek, E.K. Nyakatura, U.I.M. Gerling, S. Ye, B. Koksch, Fluorinated amino acids: compatibility with native protein structures and effects on protein–protein interactions, Chem. Soc. Rev. 41 (2012) 2135-2171.
[40] H. Welte, T. Zhou, X. Mihajlenko, O. Mayans, M. Kovermann, What does fluorine do to a protein? Thermodynamic, and highly- resolved structural insights into fluorine-labelled variants of the cold shock protein., Sci. Rep. 10 (2020) 2640.
[41] J.T. Gerig, Fluorine NMR, in: B. Society (Ed.), Biophysics Textbook Online, Biophysical Society, Bethesda MD, 2003, pp. 1-35.
[42] J.T. Gerig, Fluorine NMR of proteins, Prog. NMR. Spec. 26 (1994) 293-370.
[43] C.D. Pietrantonio, A. Pandey, J. Gould, A. Hasabnis, R.S. Prosser, Understanding Protein Function Through an Ensemble Description: Characterization of Functional States by ^{19}F NMR, Methods in Enzymology 615 (2019) 103-130.
[44] T.H. Kim, P. Mehrabi, Z. Ren, A. Sljoka, C. Ing, A. Bezginov, L. Ye, R. Pomes, R.S. Prosser, E.F. Pai, The role of dimer asymmetry and protomer dynamics in enzyme catalysis., Science 355 (2017) eaag2355.
[45] E. Matei, A.M. Gronenborn, ^{19}F paramagnetic relaxation enhancement: A valuable tool for distance measurements in proteins., Angew. Chem. Int. Ed. Engl. 55 (2016) 150-154.
[46] N.P. Chowdhury, K. Klomann, A. Seubert, W. Buckel, Reduction of Flavodoxin by Electron Bifurcation and Sodium Ion-dependent Reoxidation by NAD+ Catalyzed by Ferredoxin-NAD+ Reductase (Rnf), J Biol Chem 291(23) (2016) 11993-2002.
[47] E.H. Anderson, Growth requirements of virus-resistant mutants of *Escherichia coli* strain B, Proc. Natl. Acad. Sci. U S A 32(5) (1946) 120-128.
[48] D.C. Muchmore, L.P. McIntosh, C.B. Russell, D.E. Anderson, F.W. Dahlquist, Expression and Nitrogen-15 Labeling of Proteins for Proton and Nitrogen-15 Nuclear Magnetic Resonance, Meth. Enzymol. 177 (1989) 44-73.
[49] A. Aliverti, B. Curti, M.A. Vanoni, Identifying and quantitating FAD and FMN in simple and in iron-sulfur-containing flavoproteins., in: S.K. Chapman, G.A. Reid (Eds.), Methods in Molecular Biology, Humana Press Inc., Totowa, NJ, 1999, pp. 9-23.
[50] J.W. Hinkson, Azotobacter free-radical flavoprotein. Preparation and properties of the apoprotein., Biochemistry 7(7) (1968) 2666–2672.
[51] A. Lostao, M. El Harrous, F. Daoudi, A. Romero, A. Parody-Morreale, J. Sancho, Dissecting the Energetics of the Apoflavodoxin-FMN Complex, J. Biol. Chem. 275(13) (2000) 9518-9526.
[52] M.H. Hefti, J. Vervoort, W.J. van Berkel, Deflavination and reconstitution of flavoproteins. Tackling fold and function., Eur. J. Biochem. 270 (2003) 4227-4242.
[53] A.S. Abramovitz, V. Massey, Interaction of phenols with old yellow enzyme, J. Biochel. Chem. 251 (1976) 5327-5336.
[54] L.C. Seefeldt, S.A. Ensign, A continuous, spectrophotometric activity assay for nitrogenase using the reductant titanium(III) citrate., Anal. Biochem. 221 (1994) 379-386.
[55] J.C. Arents, M.A. Perez, J. Hendriks, K.J. Hellingwerf, On the midpoint potential of the FAD chromophore in a BLUF-domain containing photoreceptor protein, FEBS Lett 585(1) (2011) 167-72.

[56] D.M. Hoover, C.L. Drennan, A.L. Metzger, C. Osborne, C.H. Weber, K.A. Pattridge, M.L. Ludwig, Comparisons of wild-type and mutant flavodoxins from *Anacystis nidulans*. Structural determinants of the redox potentials., J. Mol. Biol. 294 (1999) 725-743.
[57] A.G. Porras, G. Palmer, The room temperature potentiometry of xanthine oxidase., J. Biol. Chem. 257(19) (1982) 11617-11626.
[58] R. Uppal, C.D. Incarvito, K.V. Lakshmi, A.M. Valentine, Aqueous spectroscopy and redox properties of carboxylate-bound titanium., Inorg. Chem. 45(4) (2006) 1795-1804.
[59] T. Watanabe, K. Honda, Measurement of the extinction coefficient of the methyl viologen cation radical and the efficiency of its formation by semiconductor photocatalysis., J. Phys. Chem. 86(14) (1982) 2617-2619.
[60] J.B. Zehnder, K. Wuhrmann, Titanium(III) Citrate as a Nontoxic Oxidation-Reduction Buffering System for the Culture of Obligate Anaerobes., Science 194 (1976) 1165-1166.
[61] K. Arnold, L. Bordoli, J. Kopp, T. Schwede, The SWISS-MODEL Workspace: A web-based environment for protein structure homology modelling., Bioinformatics 22 (2006) 195-201.
[62] A. Waterhouse, M. Bertoni, S. Bienert, G. Studer, G. Tauriello, R. Gumienny, F.T. Heer, T.A.P. de Beer, C. Rempfer, L. Bordoli, R. Lepore, T. Schwede, SWISS-MODEL: homology modelling of protein structures and complexes., Nucleic Acids Res. 46(W1) (2014) W296-W303.
[63] C.K. Drennan, K.A. Pattridge, C.H. Weber, A.L. Metzger, D.M. Hoover, M.L. Ludwig, Refined structures of oxidized flavodoxin from *Anacystis nidulans*., J Mol Biol 294 (1999) 711-724.
[64] P. Quint, I. Ayala, S.A. Busby, M.J. Chalmers, P.R. Griffin, J. Rocca, H.S. Nick, D.N. Silverman, Structural mobility in human superoxide dismutase., Biochem. 45 (2006) 8209-8215.
[65] I. Gudim, M. Lofstad, W. van Beek, H.-P. Hersleth, High-resolution crystal structures reveal a mixture of conformers of the Gly61-Asp62 peptide bond in an oxidized flavodoxin from *Bacillus cereus*., Prot. Sci. 27 (2018) 1439-1449.
[66] J.L. Kitevski-LeBlanc, R. Evanics, R.S. Prosser, Approaches for the measurement of solvent exposure in proteins by 19F NMR, J. Biomol. NMR 45 (2009) 255-264.
[67] A. Carrington, A.D. McLachlan, Introduction to magnetic resonance., Chapman and Hall, U.S.A., 1979.
[68] P. Zhang, Nitroreductase: evidence for a fluxional low-temperature state and its possible role in enzyme activity, 2007, Doctoral Thesis, Chemistry, University of Kentucky.
[69] C. Zhao, C. Anklin, N.L. Greenbaum, Use of ^{19}F NMR methods to probe conformational heterogeneity and dynamics of exchange in functional RNA molecules, Meth. Enzymol. 549 (2014) 267-285.
[70] I. Solomon, Relaxation processes in a system of two spins., Phys. Rev. 99 (1955) 559-565.
[71] J. Anglister, T. Frey, H.M. McConnell, Distances of tyrosine residues from a spin-label hapten in the combining site of a specific monoclonal antibody., Biochem. 23(22) (1984) 5372-5375.
[72] W. Watt, A. Tulinsky, R.P. Swenson, K.D. Watenpaugh, Comparison of the crystal structures of a flavodoxin in its three oxidation states at cryogenic temperatures., J. Mol. Bio. 218 (1991) 195-208.
[73] W.W. Smith, R.M. Burnett, G.D. Darling, M.L. Ludwig, Structure of the semiquinone form of flavodoxin from *Clostridum* MP., J. Mol. Biol. 117(1) (1977) 195-225.
[74] I. Nogués, L.A. Campos, J. Sancho, C. Gómez-Moreno, S.G. Mayhew, M. Medina, Role of neighboring FMN side chains in the modulation of flavin reduction potentials and in the

energetics of the FMN:apoprotein interaction in *Anabaena* flavodoxin., Biochem. 43 (2004) 15111-15121.
[75] J. Vervoort, W.J. van Berkel, S.G. Mayhew, F. Müller, A. Bacher, P. Nielsen, J. Legall, Properties of the complexes of riboflavin 3',5'-bisphosphate and the apoflavodoxins from *Megasphaera elsdenii* and *Desulfovibrio vulgaris*., Eur. J. Biochem. 161 (1986) 749-756.
[76] B.J. Stockman, W.M. Westler, E.S. Mooberry, J.L. Markley, Flavodoxin from *Anabaena* 7120: Uniform nitrogen-15 enrichment and hydrogen-1, nitrogen-15, and phosphorus-31 NMR investigations of the flavin mononucleotide binding site in the reduced and oxidized states., Biochem. 27 (1988) 136-142.
[77] H.D. Franken, H. Rüterjans, F. Muller, Nuclear magnetic resonance investigation of N-15-labeled flavins, free and bound to *Megasphaera-elsdenii* apoflavodoxin., European Journal of Biochemistry 138(3) (1984) 481-489.
[78] M.R. Seyedsayamdost, S.Y. Reece, D.G. Nocera, J. Stubbe, Mono- di-, tri and tetra-substituted fluorotyrosines: new probes for enzymes that use tyrosyl radicals in catalysis, J. Am. Chem. Soc. 128 (2006) 1569-1579.
[79] W. Liu, P.F. Flynn, E.J. Fuentes, J.K. Kranz, M. McCormick, A.J. Wand Main chain and side chain dynamics of oxidized flavodoxin from cyanobacterium Anabaena., Biochem. 40 (2001) 14711-14753.
[80] A. Hrovat, M. Blümel, F. Löhr, S.G. Mayhew, H. Rüterjans, Backbone dynamics of oxidized and reduced *D. vulgaris* flavodoxin in solution., J. Biomol. NMR 10 (1997) 53-62.
[81] I. Perez-Dorado, A. Bortolotti, N. Cortez, J.A. Hermoso, Structural and Phylogenetic Analysis of Rhodobacter capsulatus NifF: Uncovering General Features of Nitrogen-fixation (nif)-Flavodoxins . Int. J. Mol. Sci. 14(1) (2010) 1152-1163.
[82] S.T. Rao, M. Sundaralingam, Structure of the oxidized long chain flavodoxin from Anabaena 7120 at 2 Angstroms resolution., Prot. Sci. 1 (1992) 1413-1427.
[83] K.M. Kean, R.A. Carpenter, V. Pandini, G. Zanetti, A.R. Hall, R. Faber, A. Aliverti, P.A. Karplus, High-resolution studies of hydride transfer in the ferredoxin:NADP+ reductase superfamily, FEBS J. 284 (2017) 3302-3319.
[84] D.A. Hall, C.W. Van der Kooi, C.N. Stasik, S.Y. Stevens, E.R.P. Zuiderweg, R.G. Matthews, Mapping the interactions between flavodoxin and its physiological partners flavodoxin reductase and cobalamin-dependent methionine synthase., Proc. Nat. Acad. Sci. U S A 98 (2001) 9521-9526.
[85] H.B. Gray, J.R. Winkler, Hole hopping through tyrosine/tryptophan chains protects proteins from oxidative damage, Proc Natl Acad Sci U S A 112(35) (2015) 10920-10925.
[86] A.V. Crain, J.B. Broderick, Flavodoxin cofactor binding induces structural changes that are required for protein-protein interactions with NADP+ oxidoreductase and pyruvate formate-lyase activating enzyme., Biochim Biophys Acta 1834(12) (2013) 2512-2519.